中國機械工程學刊第四十一卷第四期第 479~491 頁(民國一百零九年)
Journal of the Chinese Society of Mechanical Engineers, Vol.41, No.4, pp 479~491 (2020)

Effect of Geometric Parameters of Part Span Damper on Aerodynamic Operation in a Transonic Turbomachine

Jalalifar Mahdi*, Fallah Saleh**and Ghadiri Dehkordi Behzad***

Keywords： Transonic turbomachine, Part span damper, Shock induced separation, Vortex pattern.

ABSTRACT

Decreasing compressor weight is one of the important purposes of aero-engine high speed compressor design. A common way to achieve this is to increase the pressure producing capability of the individual stages. The usual method is to use of a high aspect ratio blade. These long and thin blades are exposed to severe vibrations in the high speed fluid flow because of the aeroelastic instability. In order to decrease these destructive vibrations, mechanical designers link adjacent blades by part span dampers. These dampers cause flow blockage and a loss in turbomachine's performance. In this study, the effect of dampers on turbomachine aerodynamic operation is investigated. Nature of Flow is steady state until near stall, thus, simulations performed assume steady state conditions. In the previous studies, little attention has been given to the effect of dampers on blade shocks and trailing edge vortices. On the other hand, the damper effect on the formation and behavior of shock induced separation has been investigated in both cases. The results show that the presence of dampers cause a decrease in isentropic efficiency. Efficiency drops with reduction in the distance between damper's leading edge and blade's leading edge, increasing damper's leading edge radius, and increasing damper thickness.

INTRODUCTION

Modern aircraft engines use high pressure ratios to increase the efficiency and to reduce losses.

Paper Received August, 2018. Revised Sepfember, 2019, Accepted October, 2019, Author for Correspondence: Jalalifar Mahdi.

**MSc. Department of Mechanical Engineering, Tarbiat Modares University (TMU), Tehran, Iran.*
*** PhD, Department of Mechanical Engineering, Tarbiat Modares University (TMU), Tehran, Iran*
****Associate Professor, Department of Mechanical Engineering, Tarbiat Modares University (TMU), Tehran, Iran.*

In order to achieve the higher ratio, the number of compressor stages is increased leading to an increase in the weight of the compressor and engine. To minimize this weight impact, the pressure producing capability of the individual stages is increased and short chord (high aspect ratio) blades are used. The latter method leads to blade rotation at very high rates. The lower natural frequencies associated with these blades lead to resonated vibrations in the vicinity of these frequencies. It is necessary to control these frequencies and their mode shapes without significantly affecting the overall weight of the blades. This can be done by either changing the blade material or introducing part span dampers on the blades. The former can be very costly. On the other hand, devices like dampers introduce additional weight. Despite the benefit of the dampers to reduce or eliminate destructive vibrations, they dampers can have negative impacts on the aerodynamic performance of the turbomachines and engines.

Benser et al. (1975) has examined the aerodynamic impact of dampers by using a laser hologram in the vicinity of the damper. Her results indicate that in addition to the passage shock wave created by the blade leading-edge, there are two other shock waves created by the presence of the dampers. The first starts from the damper leading edge of the blade suction surface and the second arises from the junction of adjacent dampers with both propagating radially toward the tip.

Reid and Urasek (1973) showed that the strength of the shock related to the rotor blades depends on the relative thickness of the leading edge for any given Mach number while the strength of the second damper related shock depends on the mismatch of the bearing surfaces for various running speeds and as such would be very difficult to assess.

Esgar and Sandercock (1973) demonstrated that the performance of the rotor can be predicted if the total pressure loss distribution in the region of the damper is known. They took measured values of energy addition and loss from transonic compressors with dampers and used these data to calculate the variations in outlet air velocity and pressure over the blade span. This data is then correlated with certain aerodynamic and geometric parameters to give an approach of predicting the localized damper influence during the design phase. Roberts (1979) obtained a correlation between part span damper losses and blade geometric data. In this study, 21 transonic axial flow rotors had been used that varied greatly in tip speed and loading.

Wu et al. (2011) used an optimization method to minimize the drag force caused by the part span dampers, while maximizing the structural life of the blade. The performance of the low pressure steam turbine with different mid-span dampers was examined by Liu et al. (2011) in Ansys CFX with the results showing that a cylindrical mid span damper reduces the efficiency by 0.32 percent. The presence of PSC causes the cross flow from pressure side to suction side of bucket to roll up in the form of vortex. This leads to aerodynamic losses and deficit in work extraction. PSC is obstruction to flow and it has adverse effect on the aerodynamic performance.

Denton (1993) has studied the losses when entropy increases. Entropy's growth can be obtained using the simple summation of increases in entropy throughout the machine. Wadia and Szucs (2008) have reported numerical results for differences in aerodynamic performance caused by the presence of part span dampers in the fan blades.

Hafele et al. (2014) have studied effect of part span dampers on aero-thermodynamics in wet steam flow. This has considered the blockage of steam flow due to the part span damper within the blade channel. Detailed flow field analyses and a comparison of blade loading between configurations with and without part-span shrouds are presented in this paper. The results show significant interaction of the cross flow vortex along the part-span shroud with the blade passage flow causing aerodynamic losses (Hafele et al. 2015).

Mistry et al. (2011) studied on steam turbine blades with part span dampers. The result of this investigation showed a drop in efficiency of about 0.32 percentage points. Maier et al. (1985) worked on cylindrical damping in a steam turbine. Efficiency drop was measured almost two percentage points. Markus Hafele et al. (2015) have numerically optimized aerodynamic of part span dampers in last stage of a low-pressure industrial steam turbine. They focused on last stage rotor because these blades are strongly twisted and tapered. The results of this study show that the loss depends on the blockage area. The value of these losses are between 2.5% and 5%. They have realized that a change of shape from circular to elliptical reduces additional loss.

Acceptable aerodynamic and aeroelastic behaviors of turbomachine blades with part span dampers, depend on the optimum design of geometry and location of part span dampers.

In this paper, identification and comparison of flow behaviors on the blade are simulated and compared with and without dampers. The effect of geometric parameters on aerodynamic operation for turbomachine near stall is also investigated. Because of the transonic regime in the assumed engine, shock and boundary layer interaction occurs. The novelty is the parametric study and also considering effect of each parameter on near stall. Therefore, prior to an investigation of damper effect on the rotor operation, shock behavior and its effects on entropy and drag are studied. Then, the impacts of dampers on aerodynamic are investigated and the reason of each phenomenon is explained. In the next section, the effect of damper geometry on flow behavior is investigated using numerous simulations. In this study, a wide range is assumed for each geometric parameter to cover all possible flow behaviors for optimization purposes. The effect of geometric parameters on damper losses is also investigated and the reason of each phenomenon is explained.

Part span dampers, have been used for many years, and are still actively used due to their benefit in reduction of blade vibrations. This work presents precise knowledge about flow around the dampers and blades and provides designers with a valuable tool to forecast impact on aerodynamics with each geometric change.

METHODOLOGY

Case configuration

In the present study, the simulations have been performed on the General Electric *J85-GE-21* engine, with a transonic axial-flow compressor rotor. It has 25 blades, a designed rotary speed of 1741 Rad/Sec, mass flow rate of 24.1 kg/sec, and nominal efficiency of 85%. Figure 1 shows the geometry of its blade.

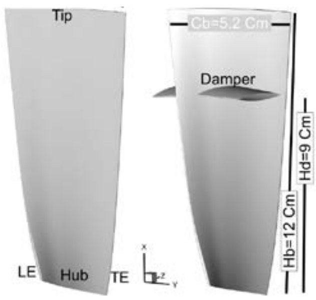

Fig.1. Blade geometry; with and without damper

Khaleghi 2015 suggests that the axial extension of the domain upstream of the rotor is four times larger than the tip axial chord and the downstream boundary is eight times larger than the tip axial chord downstream. At the inlet boundary, the standard conditions for the total pressure and temperature are specified. The turbulence intensity at the inlet boundary is five percent. At the outlet boundary, the static pressure is specified. In order to reduce total mesh and computational time, one blade channel is considered by using periodic conditions for the lateral surface of the domain. Surfaces of the hub, shroud, and blade are treated as the walls with no slip condition.

Numerical Method

The three-dimensional, steady state, and fully turbulent numerical studies are carried out on the first stage of a high pressure compressor with and without part-span dampers to examine their impact on aerodynamic. ANSYS CFX 16.2 has been employed to calculate the flow field. The three-dimensional Navier–Stokes equations are solved in a rotating reference frame, using a finite volume approach. Steady state flow is assumed as long as no periodic oscillations are observed in computational residual. These oscillations are observed in the near stall condition, therefore, the steady state assumption is considered for all simulations in this study. The equations for conservation of mass, momentum, energy and state, are mentioned in Fluent User's Guide.

For flows within turbomachines, the Reynolds number generally is high and the flow is turbulent with an extremely small time Scale. Therefore, in this study, pseudo time scale is set as 0.0001 and $k-\omega\, SST$ turbulence model is used. Detail formulations of this turbulence model are explained in the references Menter 1994.

Validation

The transonic compressor Rotor 37 is used as a test case to validate the 3-D CFD solver and the solution process. This rotor was designed and tested by Reid and Moore 2001. As a validation of the CFD solver for a 3-D compressor, the steady state solution of Rotor 37 is calculated. The representative values for this rotor are shown in the paper of Houghton and Day 2011. The boundary condition is similar to the present work as stated earlier. A grid with 1.8 million elements is enough and satisfies the mesh independency criterion.

With this grid, the chocking mass flow rate is obtained by increasing the outlet static pressure. Numerical chocking mass flow for rotor NASA 37 is 21kg/s and 20.98 kg/s for the experimental and the present work respectively. The computed and experimental mass flow rates have been normalized by using their respective choking mass flow. As shown in Figure 2, numerical efficiency underestimates experimental efficiency.

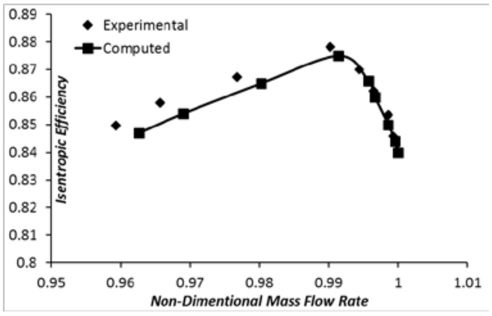

Fig.2 Variations of efficiency versus non-dimensional mass flow rate for NASA 37 Rotor.

Figures 3, 4 and 5 show the Mach contour of the 70 percent span section and it can be seen that the bow shock and the shock/boundary layer interaction around leading edge is appeared. Figure 5 is regard to current study. Comparison this Figure with experimental and numerical works (Figures 3 and 4) is evidence for validation of this work.

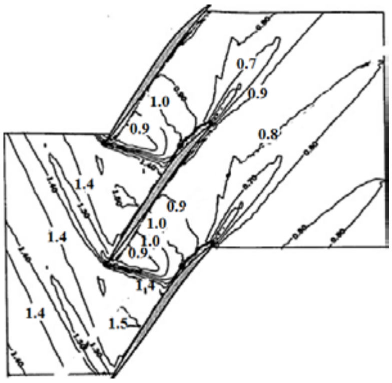

Fig.3. Mach contour at experimental investigation for NASA37 (Ameri 2011).

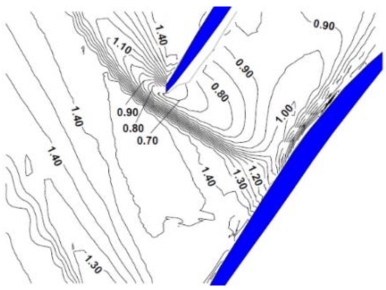

Fig.4. Mach contour at numerical investigation for NASA37 (Suder 1998).

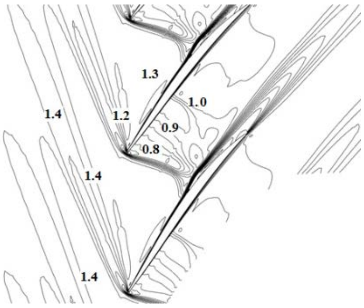

Fig.5. Mach contour at numerical investigation for NASA37 (current study).

Mesh study

Grid generation with structured mesh on complex damper geometries is a challenging and time consuming task during the design phase. In order to generate a reliable mesh on the blade especially in the damper region, ANSYS ICEM 16.2 has been chosen.

A multiblock grid system for single blade passage computation is generated as follows: 18 blocks are placed around the blade, and 6 blocks are generated in the tip clearance region. Blocks around the blade consist of 60×103×20 nodes, whereas blocks in the tip region consist of 60×17×20 nodes and blocks around each damper feature 18×10×50 nodes. A rigorous grid study was carried out to identify the correct grid resolution to get an accurate CFD model for the rotor. The computed rotor efficiency for coarse and fine mesh near the nominal conditions is shown in Figure 6. It reveals that increasing the number of elements beyond 1.4 million, does not change the efficiency significantly. Mesh density is also important and will be discussed in the next section.

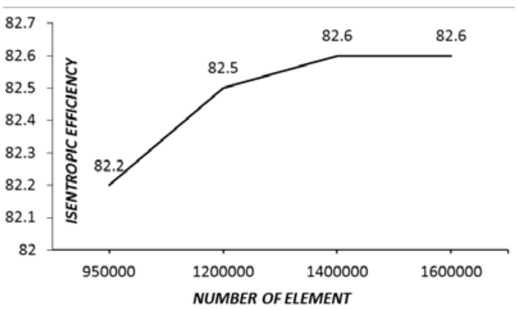

Fig.6 Variation of Isentropic efficiency versus number of elements for current study rotor

Boundary layer mesh

Assessment of y+ or the dimensionless wall distance is the best method to specify the refinement of the grid in the boundary layers. In the present study, y+ values are between 10 and 20 near the blade walls and approach the value of 20 near the damper walls. This range satisfies appropriate values in $k-\omega\, sst$ turbulence modeling (Camara 2015). The y+ values at the tip shroud and around the dampers are shown in Figures 7-a, and 7-b respectively.

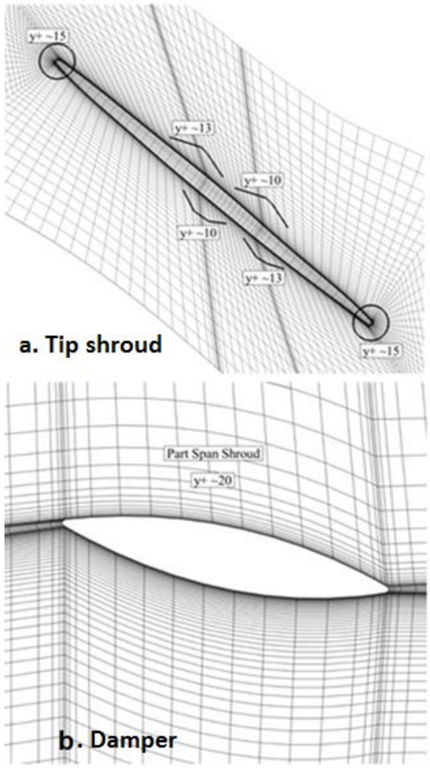

Fig.7. y^+ value in the vicinity of the blade and damper

EFFECT OF DATUM DAMPER CONFIGURATION

Performance comparison

As the outlet static pressure decreases, mass flow and therefore axial velocity increase. This trend continues until mass flow reaches a critical value in which further increase in mass flow through the blade passage is not possible. At this point, the flow in the rotor starts to choke and a sharp decrease in pressure ratio and an increase in losses occur. The mass flow rate for outlet static pressure for blade with and without dampers is plotted in Figure 8. As shown, in a rotor without blade dampers, mass flow is 22.925 kg/sec at an outlet static pressure of 80000 Pa. In a rotor with blade damper, mass flow rate is 23 kg/sec at 85000 Pa of outlet pressure.

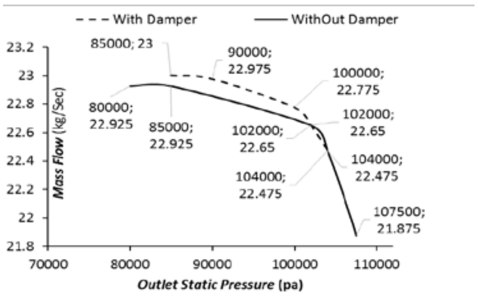

Fig. 8. Variation of mass flow rate versus outflow pressure

Since the current compressor is transonic, increasing in flow density is possible. As seen in Figure 9, model with part span shroud (PSS) has higher density than the without PSS one, on the other hand, the section area is decreased by damper and moreover, velocity chart shows velocity increases for model with PSS. These changes preserve to end of blade. Therefore, mass flow that is produced of density, area, and velocity increases for model with PSS.

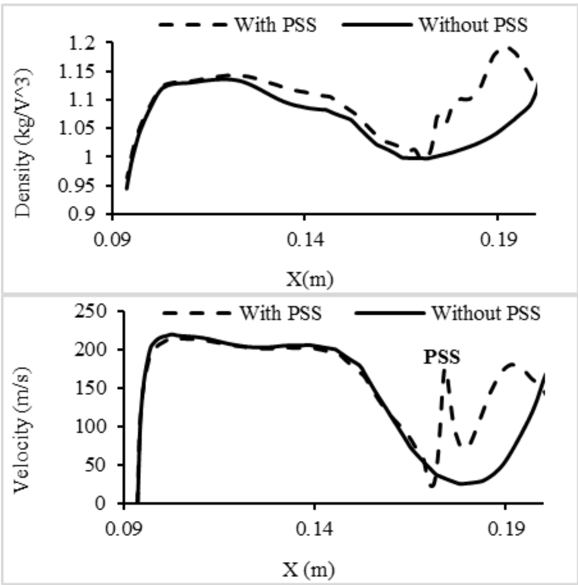

Fig.9. Variations of density and velocity at the blade trailing edge for blades with and without damper.

Figures 10 and 11 demonstrates that reduction of non-dimensional mass flow or increase static pressure causes increasing relative total pressure and efficiency until is approached to near stall.

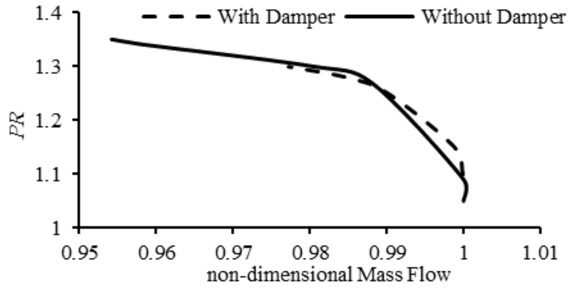

Fig.10. Variations of efficiency versus non-dimensional mass flow rate (Present Study)

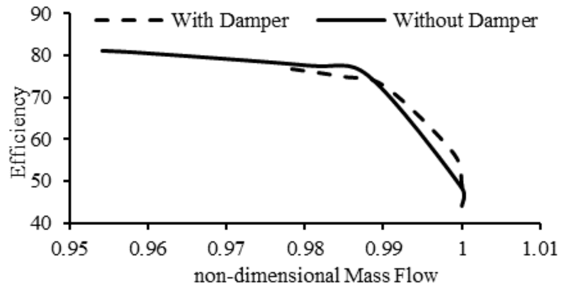

Fig. 11 Variations of total pressure ratio versus non-dimensional mass flow rate (Present Study)

Figure 12 showed outlet total pressure for blades with and without dampers. The results showed that the pressure abruptly decreases near the damper. Total pressure reduction is another factor that leads to decreasing efficiency.

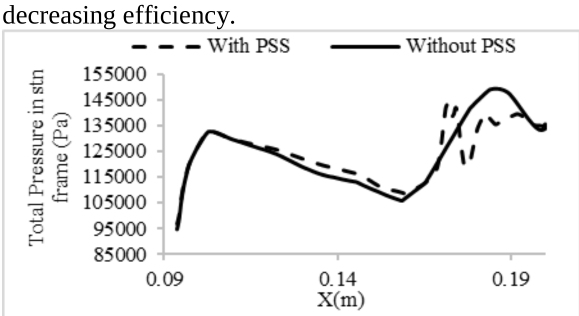

Fig.12 Variations of outlet total pressure in stn frame at blade trailing edge for blades with and without damper.

FLOW FIELD COMPARISON

Blade shock pattern

Transonic fan and compressor rotor blade rows operate in the supersonic regime over a large part of the blade span. Blockage of flow by blade and velocity diffusion combined with supersonic inlet relative velocities lead to strong shockwaves in the blade tip regions (Figure 13a). After the first shock, the velocity is decreased, but due to decreasing section area, the velocity and Mach number are increased. The second blade shock appears in the middle of the blade (throat) approximately. Figure

13b shows that the second shock on the blade surface extends from hub to tip. The first shock starts from mid-span (x≈17cm) and the second shock exists from near hub to near tip shroud.

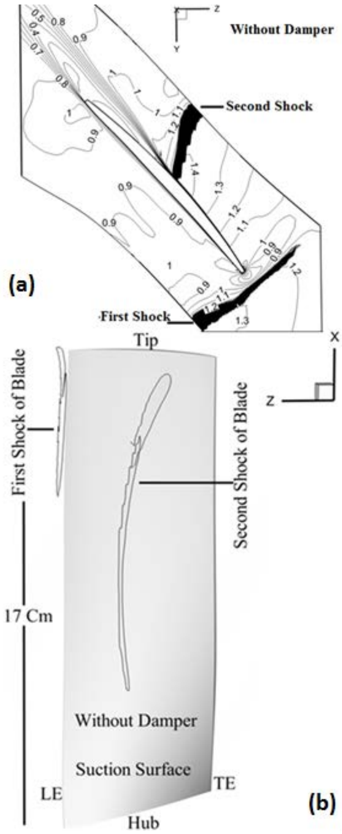

Fig.13 Investigation shocks on the surface

Benser [1] observed a shock that appears in the leading edge and two shocks due to the dampers (Figure 14). These works have specified that two shocks appear for blade in leading edge and middle chord of the blade and there is a shock due to damper.

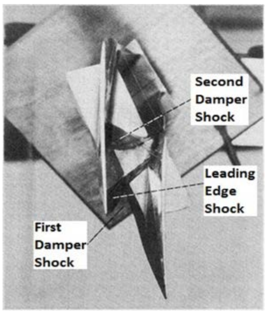

Fig.14. Shocks of the blade with damper (Benser et al. 1975)

Shock wave/boundary layer interaction (SBLI) appears usually in transonic or supersonic flows, and involves almost all types of fluid dynamic phenomena. Of the many aspects of SBLI phenomena, Shock Induced Separation (SIS) is the most important as it has a deterministic influence on the overall flow characteristics. When the shock wave interacts with the boundary layer flow, many diverse types of flow phenomena occur: flow separation, unsteadiness, vortical flow, pressure waves, complicated mixing, turbulence, etc. It has four patterns: weak, moderate, strong, and very strong (Setoguchi 2007). Figure 15 shows SBLI and increasing in entropy caused by this interaction. Vorticity at the blade trailing edge that is formed due to the interaction.

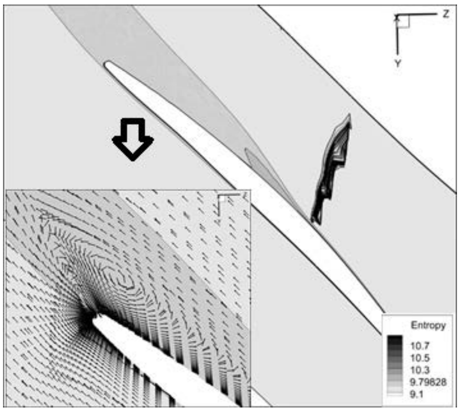

Fig. 15 increasing entropy due to SBLI

Effect of damper on shocks

The flow field for the rotor operation at design speed is presented in terms of Mach number and shock contours in Figure 16. This Figure is regarded to blade with damper which install at 75% span. Figure 16a and 16b feature flow field at 80% and 85% of the span respectively. In comparing Mach numbers in Figures 16a and 13a specific that damper doesn't have effect on the second shock strength of the blade. In both of Figures is observed that Mach number is dropped from 1.3 to 1.1. Figure 16b shows that, second blade shock doesn't appear on top of the damper. In this region just damper shock is created.

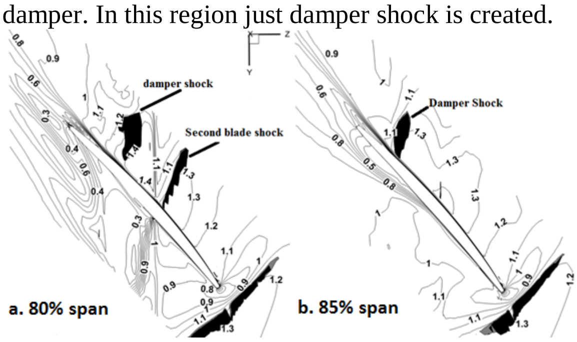

Fig. 16 Contour Shock and Mach for blade with part span damper

Effect of Losses on entropy

According to Wilson and Korakianitis 1998, a real compressor can be thought of as an ideal machine taking in a gas at P_{in}, h_{in} and outputting it at P'_{out}, h'_{out} (ideal state) and at P_{out} , h_{out} with losses considered, which make the actual delivery conditions. An isentropic enthalpy rise is followed by a pure entropy increase, which shows the entropy generated is because of the internal losses. Isentropic efficiency is defined by equation 1 (Wilson, Gordon 2002). This simplifies to equation 2 assuming ideal gases.

$$\eta_c = \frac{h'_{out} - h_{in}}{h_{out} - h_{in}} \qquad 1$$

$$\eta_c = \frac{\left(\left(\frac{P_{tot,Out}}{P_{tot,In}}\right)^{\lambda-1/\lambda}\right) - 1}{\left(\frac{T_{tot,Out}}{T_{tot,In}}\right) - 1} \qquad 2$$

And also, isentropic efficiency and entropy are equivalent with each other:

$$\eta = 1 - \frac{T_t \ \Delta S}{\Delta h_t} \qquad 3$$

With addition of losses, entropy increases and, therefore, efficiency decreases. Efficiency has been predicted by comparison of entropy contours for different dampers.

As Figure 17 shows, entropy rises past the damper trailing edge. Entropy on the suction surface depends on shock at this surface, whereas, entropy on pressure surface above the damper is high due to the effect of the damper. According to Esgar and Sandercock (1973) and Roberts 1979, the effect of part span dampers is mostly confined to ±5% and ±15% of span from its location respectively. It is similarly evident in this study that the entropy rise due to the damper's presence decreases with increasing distance from the damper region.

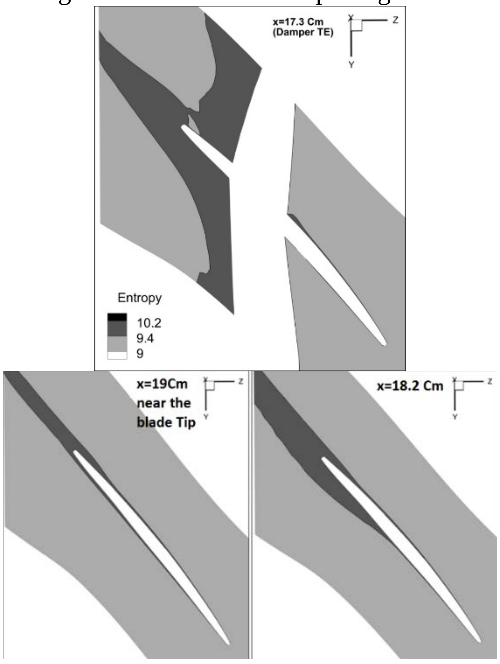

Fig.17 Entropy distribution

PARAMETRIC STUDY

In this section, values of geometric parameters are varied independently one at a time with the remaining parameters remaining constant and their effect on aerodynamic operation is investigated. During the modeling, outlet total pressure is assumed to be constant and its amount is 102000 Pa.

Chord-Wise position (distance between damper and blade)

Figure 18 shows variation in damper location along blade.

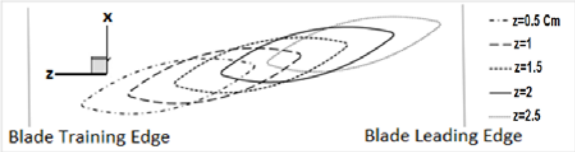

Fig.18 Variation of distances between blade leading edge and damper leading edge

As Figure 19 depicts, increasing the distance between blade leading edge and damper leading edge, leads to reduction in entropy and therefore increase in efficiency.

Figure 20 also confirms this prediction. Esgar and Sandercock (1973) have shown that damper losses decrease as the damper is moved further away from the blade leading edge.

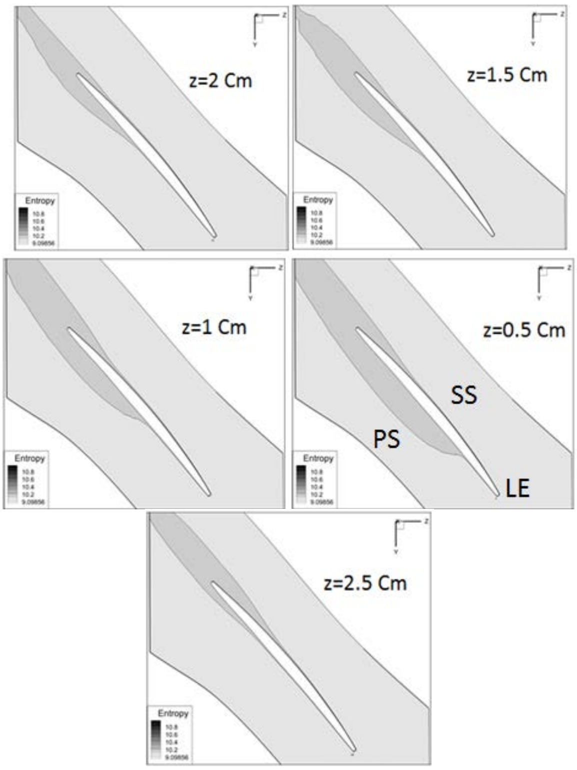

Fig.19. decreasing entropy with increasing z

parameter

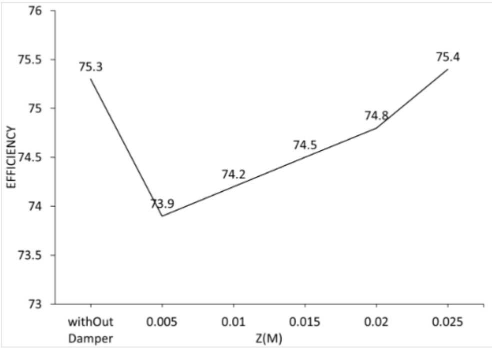

Fig.20 Efficiency versus z parameters

According to Figure 21a, if the damper is placed near the blade's leading edge, shock appears in two regions: one extends from the hub to near the damper with its associated shock being due to the blade and the second damper related shock extends from above damper outwards. Total shock on the blade decreases and hence this decrease of shock wave indicates wave drag and, therefore, total drag of the rotor is decreased (Figure 22). With the damper located away from the blade's leading edge, the second shock of the blade propagates to the tip region giving a rise to the drag force. Yuan- Ting Wu 2011 has shown this phenomenon via the optimization approach. Figure 21b shows the elongated propagation of the shock with a 'z' value of 2.5cm.

Figure 24 shows the velocity vector on the damper surface and shock contour above it. As seen, for a z value of 0.5cm a small amount of vorticity forms, but it is small and with a small SBLI also, the total drag force is relatively low. On the other hand, with a z value of 2cm, both SBLI and vorticity are large and consequently the total drag is relatively high. For z=2.5cm, SBLI and wave drag don't occur, but the big vorticity formed at the damper trailing edge results in high pressure drag.

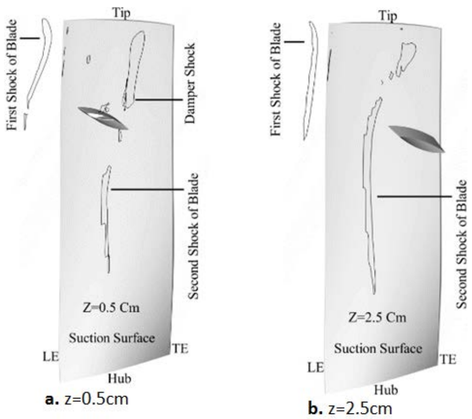

Fig.21. Shock radial propagation for z=0.5 Cm

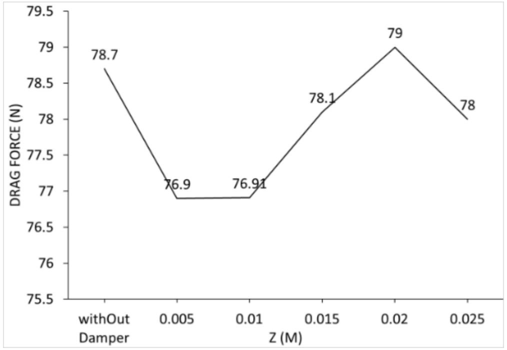

Fig. 22. Variation of total drag for different z values

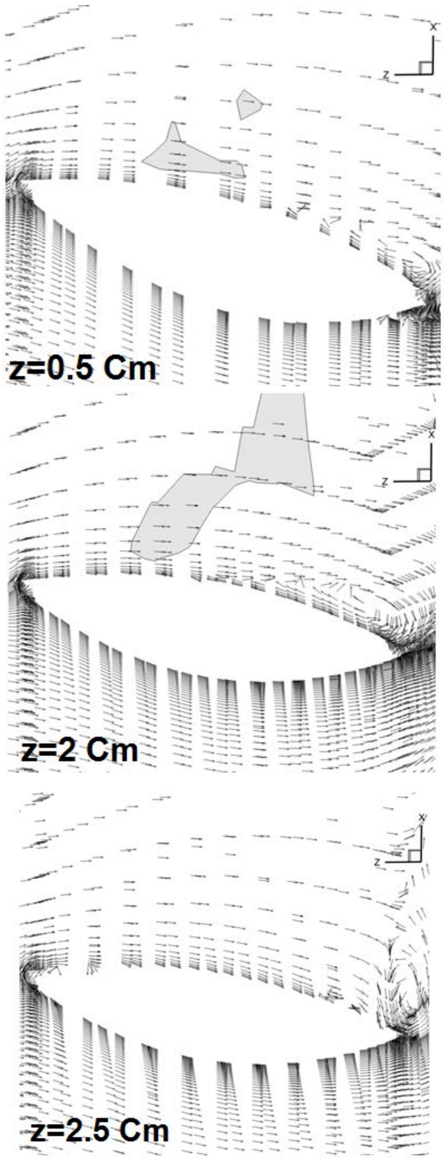

Fig. 23 Velocity vector on the damper surface and shock contour above it

Leading edge radius

Fig. 24 shows variations in damper leading edge radius. The initial radius is 0.015 cm and other radii are multiples of that.

Fig.24**.** variation of damper leading edge radius

Figure 25 shows the velocity vectors on the damper along with the shock contours. Wadia and Szucs (2008) concluded that the shock-boundary layer interaction seems to be improved when dampers are present. In this study, this claim is investigated. Distance between damper's suction surface and shock tip is rises as the leading edge radius increases. For this discussion, R represents the initial damper's leading edge radius. Shock appears near the surface of the damper, resulting in high wave drag. Velocity vector in Fig. 25 shows that when damper's leading edge radius is increased, area with adverse velocity gradient increases but separation doesn't occur. Consequently, pressure drag doesn't exist. In order to decrease wave drag, damper's leading edge radius shouldn't be very high. If the damper's leading edge radius is 10R, flow separates and vorticity forms generating pressure drag. As seen in Figure 27, increasing damper's leading edge radius causes a reduction in drag, but at the radius 10R the drag has increased.

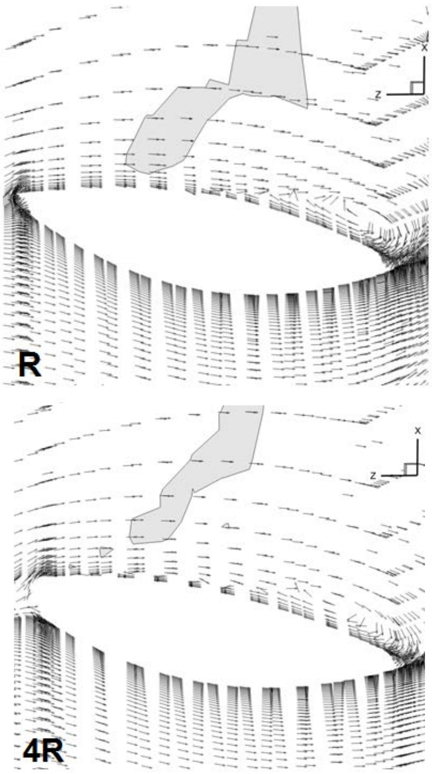

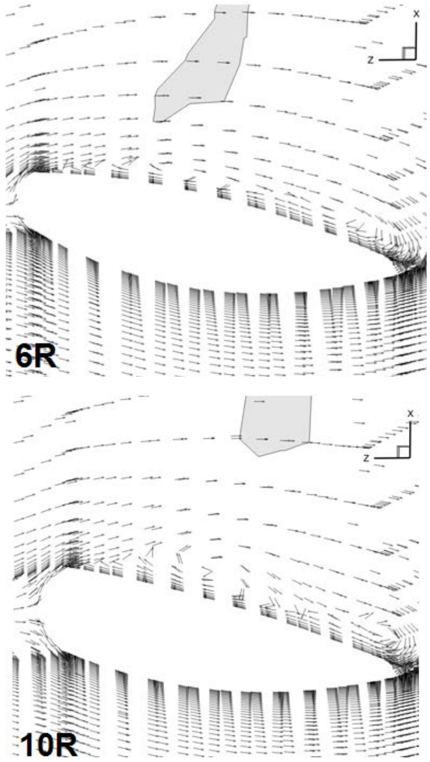

Fig.25**.** Velocity vector on the damper surface and shock above it

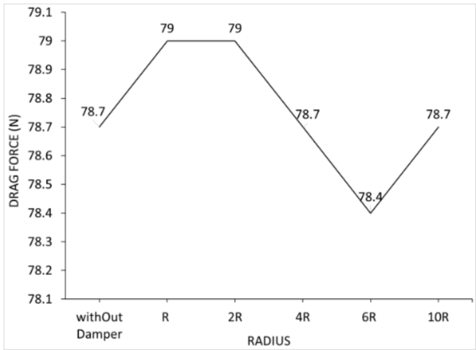

Fig.27 Total drag for different radii

It was already mentioned that with rising damper's leading edge radius, more regions have been influenced by the adverse velocity profile. For example, in radius 10R separation occurs. As a consequence, increasing damper's leading edge radius causes increasing entropy and loss and then reducing the efficiency. Fig. 27 shows a diagram of isentropic efficiency for radii R- 10R and related entropy contours.

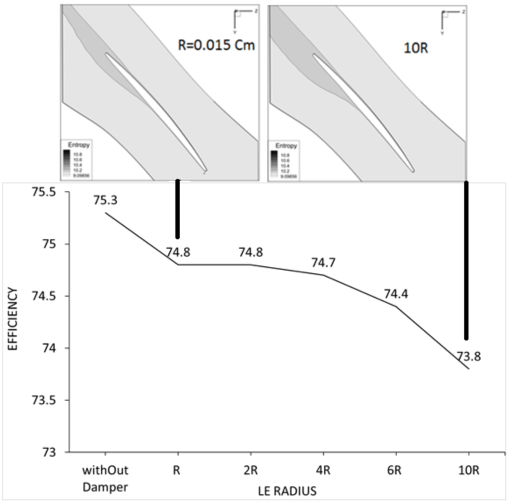

Fig.27 Variation entropy and efficiency by increasing radius

Maximum thickness

In this study, the damper maximum thickness is assumed to be a function of damper's leading edge radius. Thus, the initial value of thickness is equal to damper leading edge diameter (t=D). Figure 28 shows the variation process for damper thickness.

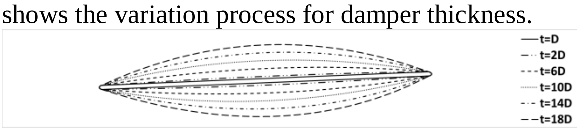

Fig.28 change in damper maximum thickness

Velocity vector on damper with thickness t=D shows that adverse velocity profile starts from near the damper's leading edge and separation occurs after that followed by formation of vorticity (Figure 29). Increasing damper thickness causes the adverse velocity profile to appear later and, therefore, separation delays reducing the total drag. At t=18D great vorticity forms after damper's trailing edge that causes a rise in total drag (Figure 30).

For t=D, separated flow recovers on the blade surface again. Also, because of the small thickness, the region of influence just involves the region above the damper. As seen in Figure 31, with increasing thickness, this effect extends to below the damper. Because of this, at t=D, entropy is similar to the blade without damper and, therefore, the efficiencies of these blades are equivalent approximately (Figure 32). Esgar and Sandercock's work indicates that, qualitatively, the magnitude of damper loss decreases with a reduction in damper maximum thickness.

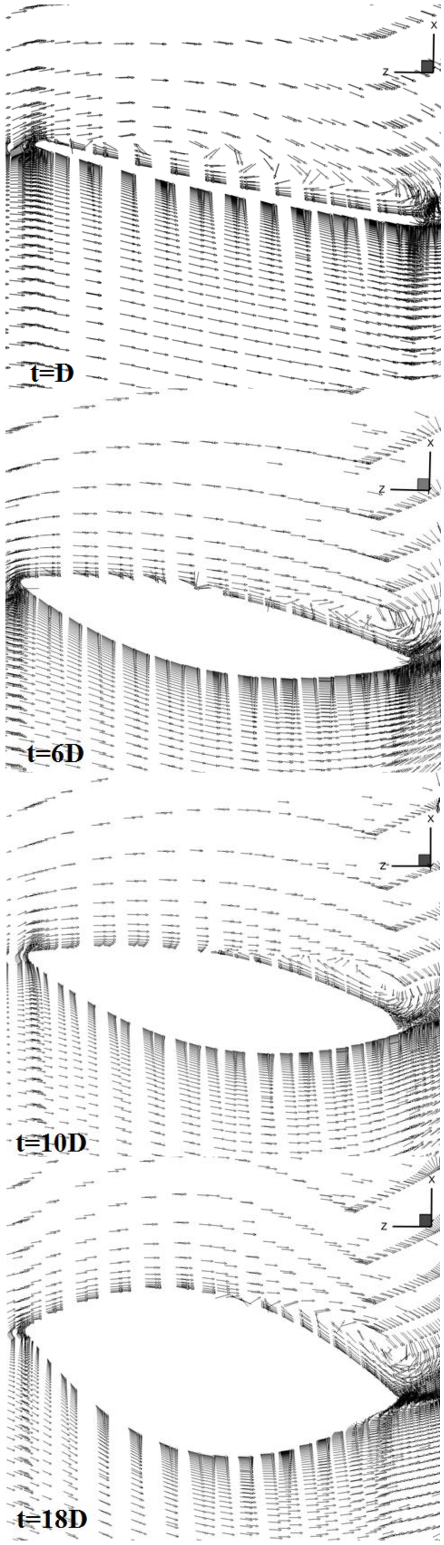

Fig.29 Velocity vector and shock for damper different thicknesses

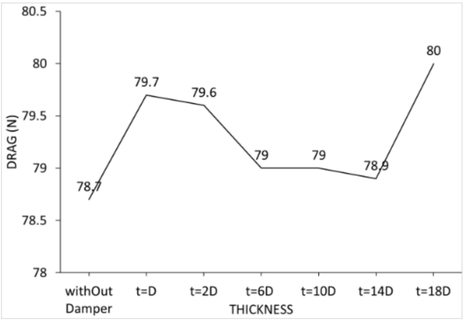

Fig.30 Variation drags with increasing thickness

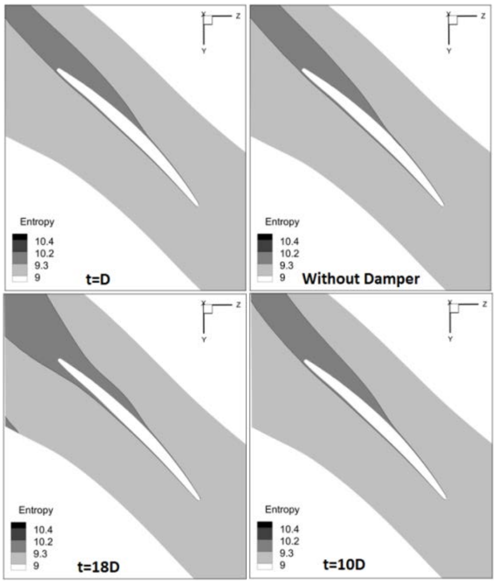

Fig.31 Entropy contour for below regions of damper

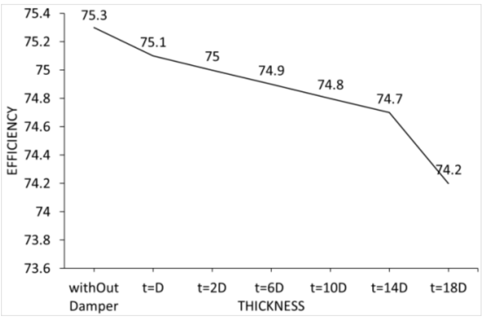

Fig.32 Process of variation efficiency with increasing thickness

ANSYS CFX is used to calculate drag of the rotor. As seen in charts, reduction in leading edge radius and thickness causes efficiency to increase and this happen because of the damper become thin. On the other hand, drag of the thin damper is higher than others. Therefore, optimization of the damper thickness and radius is necessary for the appropriate value.

Chord length

Figure 33 shows two dampers that have similar geometry parameters with different chord lengths. With decreasing damper chord length, larger vorticity is generated causing an increase in drag. Comparison of entropy contours in Figure 34 indicates that the increasing chord length causes a little increase in efficiency.

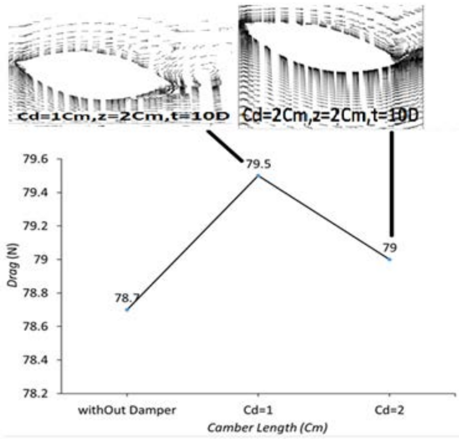

Fig.33 Effect of damper length on drag force

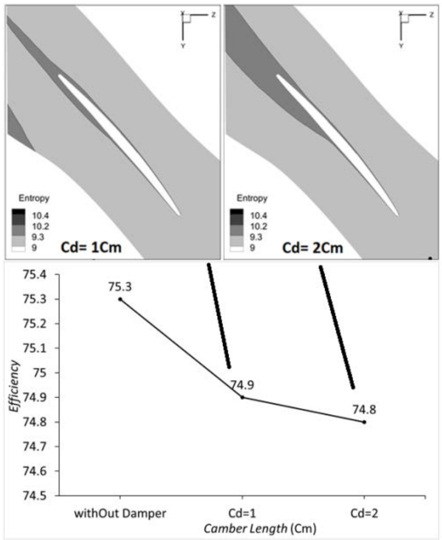

Fig.34 Effect of damper length on efficiency

Strength of shock

Plots in Figure 35 shows that variation of the geometric parameters doesn’t have effect on damper shock strength. For all models, Mach number is dropped from 1.3 to 1.1 through the shock.

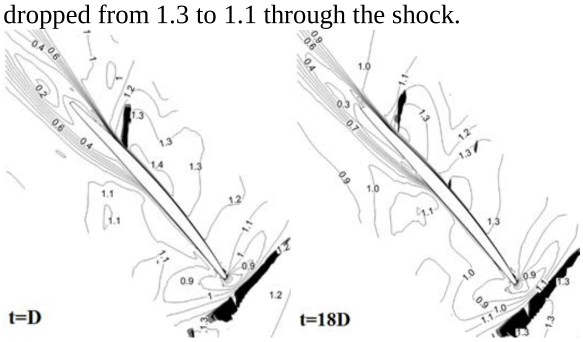

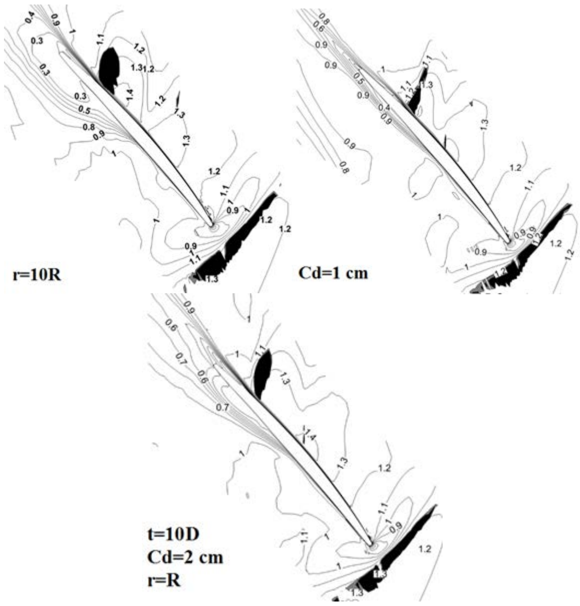

Fig.35 compression strength of shock for variable parameters

Near stall inception

Figure 36 demonstrates that how near stall condition is affected by the variation of the parameters. For rotor with damper, stall occurs at outlet total pressure 103000 Pa while for the blade without damper it is 107500 Pa. As seen, stall happens in lower outlet total pressure when thickness of the damper is more than 14 D. This happens when damper locates at place 2.5cm from blade leading edge. Rotor with damper which its chord length is 1cm, stall occurs at 107000 Pa pressure.

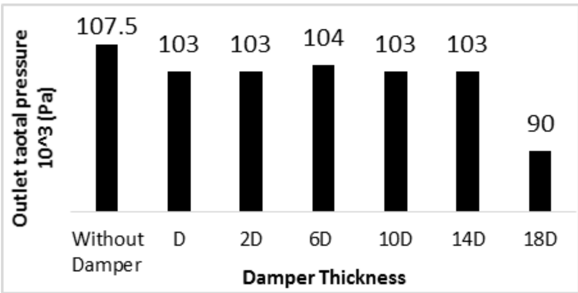

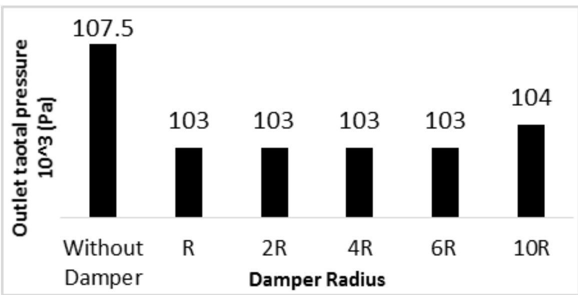

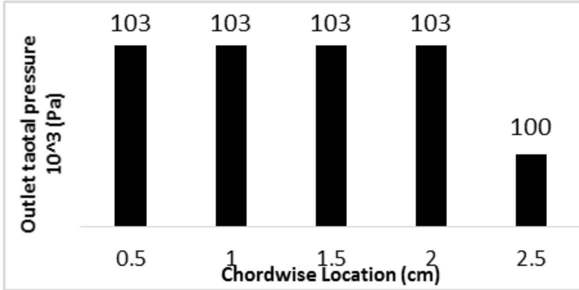

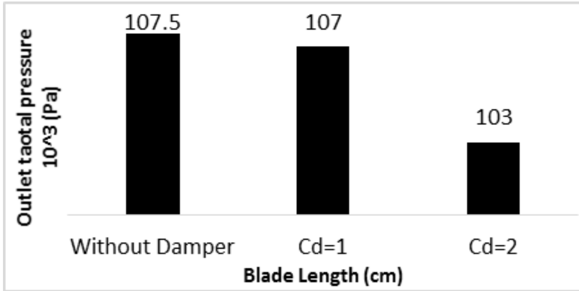

Fig.36 Comparison stall for different models

Conclusion

The most common method for increasing the pressure producing capability of the individual stage is the use of blades with high aspect ratios. In order to reduce destructive vibrations in blades; designers have connected adjacent blades with damper. In this study the effect of presence of dampers and their geometry on the aerodynamic operation of turbomachine has been studied. The results are summarized below:

1. In this compressor, shock wave/ boundary layer interaction may occur which can in turn cause a rise in entropy and formation of vorticity. This interaction may, therefore, establish unsteadiness and accelerate stall initiation. The entropy at the trailing edge of the damper is greatly increased by the damper. Entropy on top of the damper decrease. Entropy at the blade pressure surface is increased caused by damper which is near leading edge of the blade.
2. If the damper is located at the middle of the blade, damper shock appears above the damper and causes SBLI. If the damper is situated the near blade's trailing edge, there isn't a shock above the damper. An increase in damper's leading edge radius results in an increase in the distance between the shock above the damper and the damper surface.
3. Damper away from the leading edge blade cause efficiency increase. Increasing in the entropy and losses and decreasing in the efficiency is caused by increasing in the leading edge radius of damper. Decreasing the damper thickness reduces the area affected by damper, and then reduce the

efficiency.

4. Decrease in drag caused by increase in leading edge damper radius and thickness. But there is a limit for this growth of parameters. Reduction of damper's chord length increases drag.
5. With regard to charts, that is, efficiency, drag, and stall, can choose 6D as the best option for thickness.

REFERENCES

Ali Ameri. "NASA ROTOR 37 CFD CODE Validation Glenn-HT Code", *47th AIAA Aerospace Sciences Meeting including*.

Benser W.A, Bailey E. E., Gelder T. F. "Holographic Studies of Shock Waves Within Transonic Fan Rotors", *J. Eng. Power*, Vol.97, No. 1, pp. 9, Jan.1975.

Camara Enrique. "Validation of Time Domain Flutter Prediction Tool with Experimental Results", MSc Thesis, KTH School of Industrial Engineering and Management, 2015.

Denton J. D, "The 1993 IGTI Scholar Lecture: Loss Mechanisms in Turbomachines", *J. Turbomach*. Vol. 115, No.4, pp. 621-656, Oct .1993.

Esgar G. M, Sandercock D. M, "Some Observed Effects of Part- Span Dampers on Rotating Blade Row Performance near Design Point", *NASA TM X-2696*, Vol.501, No.24, pp. 28, 1973

Fluent Inc, Fluent User's Guide, 2015.

Hafele M, Starzmann J, Grubel M, et al. "Numerical investigation of the impact of part-span connectors on aero-thermodynamics in a low pressure industrial steam turbine". *ASME Paper* No. GT2014-25177, 2014.

Houghton T, Day I. "Enhancing the Stability of Subsonic Compressors Using Casing Grooves", *ASME Journal of Turbomachinery,* Vol. 133, No.2, pp. 11, April 2011.

Khaleghi H, "Stall inception and control in a transonic fan, part A: Rotating stall inception," *Aerospace Science and Technology*, Vol.41, pp. 250-258, 2015.

Liu J, Mistry H, Santhanakrishnan M, Stein A, Dey S, Slepski J. "Aerodynamic Performance Assessment Of Part-Span Connector Of Last Stage Bucket Of Low Pressure Steam Turbine," *Proceedings of the ASME 2011 Power Conference*, Vol.1, No.55265, pp. 545-550;6 pages July. 2011.

Maier R. Wirkungsgraduntersuchungen am Endstufenversuchsstand bei variierten Betriebszustanden. In: Festschrift 65. Geburtstag Prof. Dr.-Ing. Jakob Wachter, *1985, pp. 147–167*.

Markus Häfele, Christoph Traxinger, Marius Grübel, Markus Schatz, Damian M Vogt, Roman Drozdowski. "Numerical and experimental study on aerodynamic optimization of part-span connectors in the last stage of a low-pressure industrial steam turbine". *Proceedings of the Institution of Mechanical Engineers, Part A: Journal of Power and Energy*
Vol 229, Issue 5, pp. 465 - 476

Menter F.R, "Two-Equation Eddy-Viscosity Turbulence Models for Engineering Applications", *AIAA JOURNAL* Vol. 32, No. 8, August 1994

Mistry H, Santhanakrishnan M, Liu J, et al. "Aerodynamic performance assessment of part-span connector of last stage bucket of low pressure steam turbine". *ASME Paper* No. POWER 2011-55265, 2011.

Moine Y. Wu, J, Marra J. J, Ting Wu Y, Funk C. K, Hsu P. F, Zhou R, Subramanian C. S, Campbell C. X, "Design Optimization of Turbomachinery Components with Independent FEA and CFD Tools in an Optimization Software Environment - a Mid-Span Shroud Ring Study Case," *Energy Systems Analysis,* Vol.4, No. IMECE2011-62083, pp. 8, Nov. 2011.

Moore R.D, Reid L. "Performance of single-stage axial-flow transonic compressor with rotor and stator aspect ratios of 1.63 and 1.77, respectively, and with design pressure ratio of 2.05". *NASA-TP*-2001, E-334, NAS 1.60:2001. 1982.

Reid L, Urasek D. C. "Effects of Increased Leading Edge Thickness on Performance of a Transonic Blade in Single-Stage Transonic Compressor", *NASA TN* D-7489, Vol.501, No.24, pp. 56,1973 (also see ASME Paper 73-GT-60).

Roberts W. B. "A Design Point Correlation for Losses due to Part-Span Dampers on Transonic Rotors", *Journal of Engineering for Power,* VOL. 101, No.3, pp. 7, JULY 1979.

Setoguchi T, "Shock Induced Boundary Layer Separation", *8th International Symposium on Experimental and Computational Aerothermodynamics of Internal Flows*, *Lyon, France*, July-2007.

Suder KL. "Blockage Development in a Transonic, Axial Compressor Rotor". *ASME. J. Turbomach.* 1998;120(3):465-476. doi:10.1115/1.2841741.

Wadia AR, Szucs PN. "Inner Workings of Shrouded and Unshrouded Transonic Fan Blades." *ASME. J. Turbomach.* 2008; 130 (3): 031010-031010-11. doi:10.1115/1.2776957.

Wilson, Gordon David, Korakianitis T.P. "The design of high-efficiency turbomachinery and gas turbines" second edition", Prentice-Hall, Upper Saddle River, NJ. 1998, p. 358.

Wilson, Gordon David. "The basis for the prediction of high thermal fficiency in w.t.p.i. gas-turbine engines", pp. 8 , Nov. 2002.